

EBMs vs. CL: Exploring Self-Supervised Visual Pretraining for Visual Question Answering

Violetta Shevchenko¹, Ehsan Abbasnejad¹, Anthony Dick¹, Anton van den Hengel^{1,2}, Damien Teney^{1,3}

¹University of Adelaide ²Amazon ³Idiap Research Institute

[firstname].[lastname]@adelaide.edu.au

Abstract

Context. The availability of clean and diverse labeled data is a major roadblock for training models on complex tasks such as visual question answering (VQA). The extensive work on large vision-and-language models has shown that self-supervised learning is effective for pretraining multimodal interactions. In this technical report, we focus on visual representations. We review and evaluate self-supervised methods to leverage unlabeled images and pretrain a model, which we then fine-tune on a custom VQA task that allows controlled evaluation and diagnosis. We compare energy-based models (EBMs) with contrastive learning (CL). While EBMs are growing in popularity, they lack an evaluation on downstream tasks.

Findings. Both EBMs and CL can learn representations from unlabeled images that enable training a VQA model on very little annotated data. In a simple setting similar to CLEVR, we find that CL representations also improve systematic generalization, and even match the performance of representations from a larger, supervised, ImageNet-pretrained model. However, we find EBMs to be difficult to train because of instabilities and high variability in their results. We, therefore, investigate other purported benefits of EBMs. They prove useful for OOD detection, but other results on supervised energy-based training and uncertainty calibration are largely negative.

Conclusions. (1) We make the encouraging observation that self-supervised visual pretraining allows displacing some of the requirements for training data from the main/supervised to a pretraining/unsupervised stage. (2) CL currently seems a preferable option over EBMs. To our surprise, EBMs could not achieve the benefits purported in the literature, even in a toy setting.

1. Introduction

The availability of large-scale diverse datasets has been a driving force in deep learning research for computer vision as well as natural language processing (NLP). Tasks like visual question answering (VQA), that combine vision and language and involve complex reasoning, require a large amount of aligned visual and textual data for training. The generation of such data involves human annotators, making it expensive and time-consuming. Moreover, task-specific data collection from humans often introduces biases and noise in the data [40, 41] that are subsequently difficult to deal with during training [65, 66] or evaluation [14, 67].

Early methods for VQA made use of pretrained image models [2, 31] and language features [55, 60]. Most recent work has focused on pretraining general-purpose vision-and-language models [11, 49, 51, 64]. These models are pretrained with self-supervised objectives, which alleviates the need for tasks-specific VQA training examples, but they usually require aligned vision and language, such as images with captions. This motivates our exploration of self-supervised methods for pretraining the visual encoder, which only requires unlabeled images.

Our study explores the potential benefits of two popular self-supervised paradigms, energy-based models (EBMs) and contrastive learning (CL). These are applied specifically to *visual* data. Our findings are therefore particularly relevant to the training of vision-and-language models for particular visual domains (e.g. industrial or medical images) where little annotated data is available. We conduct our experiments with a simple VQA model and a custom toy task similar to CLEVR [39], which allows a controlled evaluation. Unlike most recent papers on vision and language, we do not deal with large-scale datasets nor large transformer-based models.

An important novelty of this study is the consideration of EBMs. Generative models are generally attractive in unsupervised machine learning [22, 44]. EBMs in particular have

grown in popularity [20, 24, 79] because they were shown to be also effective on discriminative tasks, with claims of improved calibration, robustness, and out-of-distribution (OOD) detection capabilities. The current literature however lacks evaluations on complex downstream tasks, which we partly remedy.

The contents of this report are summarized as follows.

1. We review the general concepts behind energy-based models (EBMs) and contrastive learning (CL).
2. We devise a simple VQA setting with data similar to CLEVR, and a simple CNN-LSTM model. Both allow a constrained and controlled evaluation, including OOD generalization (novel object/color combinations at test time).
3. In this setting, we compare EBMs with CL (SimCLR [10]) for pretraining visual representations used by the VQA model. Both methods are effective and allow training the VQA model with little annotated data. However, EBMs are practically difficult to train.
4. We compare EBMs with CL for OOD detection of images, which could serve in VQA for determining unanswerable cases at test time. EBMs are generally more reliable, but they can fail when ID and OOD data are visually similar.
5. We investigate potential benefits of supervised energy-based training of the VQA model itself, using JEM [24] and CEBM [19]. Our results are mixed, with some improvements in accuracy (at the expense of a finicky training), but none of the expected improvements in calibration.

2. Related work

Training VQA models. Visual question answering is a popular task to evaluate the progress of AI on vision and language [69, 74]. Early work on VQA trained models with supervision from question/image/answer triplets. These models (e.g. [68]) used visual features from a CNN or object detector [2] itself trained with supervision from annotated datasets such as ImageNet [15] or Visual Genome [45]. Modern approaches to VQA use large-scale transformer models trained with self-supervised objectives on vision-and-language data (e.g. [64]), before being fine-tuned with supervision of VQA triplets. The self-supervision in these models serves to learn correspondences across the visual and textual modalities, and the visual inputs are often processed by a pretrained visual encoder. Recent exceptions that appeared after our study include ViLT [43] and VLC [25], which take image patches as input, and DETR [42], X-DETR [8], SOHO [38], TxT [62]

and E2E-VLP [78], which jointly train an object detector.

Energy-based models (EBMs) offer an attractive framework to unify various areas of machine learning, and also lead to a new class of generative models. See [48] for an early tutorial. Recent studies [20, 57, 58] have investigated training techniques that enable the application of EBMs to high-dimensional data and address issues of training stability. EBMs have been applied to various areas including image generation [4, 18, 20, 29, 76, 77], graph generation [63], image classification [24], regression [27, 28], continual learning [50] and natural language processing [17, 32, 71].

Contrastive learning (CL) is one of the most popular approaches to learn representations of high-dimensional data such as images without access to training labels. A contrastive training objective essentially trains a model to differentiate between similar and dissimilar samples. While early application in computer vision [6, 30, 34, 59, 70, 75, 80] could not compete with supervised training, recent methods such as SimCLR [10] and SwAV [9] introduced novel data augmentations and architectural modifications that narrowed this gap and can now compete with the supervised paradigm. In this work, we apply contrastive learning to the visual question answering task. Another VQA method that incorporates contrastive loss was proposed by Whitehead *et al.* [73], where the model is trained on image-question pairs in a self-supervised manner. In contrast, in this work we utilize images without any additional annotations.

3. Background

The setup of our main experiments consists in pretraining a convolutional neural network (CNN) on unlabeled images with self-supervision. This CNN is then used as the visual encoder of a VQA model. The CNN is fine-tuned while training the VQA model with question/image/answer examples. With this setup, we investigate whether visual pretraining can facilitate the training of the VQA model (e.g. with less task-specific data) and/or improve its generalization capabilities. Our work does not introduce new methods besides the adaptation of EBMs and contrastive learning to the pretraining of visual representations for VQA.

This section reviews the methods used under a common technical umbrella. This background justifies the comparison of these methods in a same study and it sets the stage in terms of expectations for our experiments of Section 5.

3.1. A common self-learning objective

The self-supervised learning objective of the interest in this report can be described as:

$$\begin{aligned}\mathcal{L}_\theta(\mathbf{x}) &= -\mathbb{E}_{\mathbf{x} \sim \mathcal{D}} [\log(\tilde{p}_\theta(\mathbf{x}))], \text{ with} \\ \tilde{p}_\theta(\mathbf{x}) &= \frac{\exp(\text{score}(f_\theta(\mathbf{x})))}{Z(\theta)},\end{aligned}\quad (1)$$

where $\mathbf{x} \in \mathbb{R}^D$ is an input (unlabeled image), $f_\theta : \mathbb{R}^D \rightarrow \mathbb{R}^d$ is the neural network of parameters θ that learns a mapping from inputs to an embedding space, $Z(\theta)$ is a normalizer and \mathcal{D} is our dataset of unlabeled examples. Different choices of score function and normalizer give rise to different self-supervised learning algorithms. In particular, considering EBM [76] and the popular SimCLR [10] method for CL:

- The **score function** in EBM is learnable. It is implemented as a separate neural network that maps an embedding to a scalar that represents an unnormalized density of the input. SimCLR uses a predetermined score function. It uses the similarity of the embeddings of different views (*i.e.* semantic-preserving transformations) of the input.
- The **normalizer** in EBM is designed to ensure $\int \tilde{p}(\mathbf{x}) d\mathbf{x} = 1$. One approach to accomplish this is to estimate the normalizer using sampling, *i.e.* learning to generate samples. This is practically challenging and produces training instability. In SimCLR, rather than generating samples, augmented views of the training samples are used to compute $Z(\theta)$. The estimation of $Z(\theta)$ is simpler in SimCLR but the choice of the samples use is important.

3.2. Energy-based models

Energy-based models (EBMs) are a form of generative model that relies on an energy function to capture dependencies between the random variables to be modeled. The energy function maps each configuration of variables to a scalar energy value. It is optimized such that observed values (*i.e.* the training examples) have a low energy *i.e.* a high probability. The probability density for an input $\mathbf{x} \in \mathbb{R}^D$ is represented as

$$\text{score}(f_\theta(\mathbf{x})) = E_\theta(f_\theta(\mathbf{x})), \quad (2)$$

where $E_\theta : \mathbb{R}^d \rightarrow \mathbb{R}$ is the energy function (with abuse of notation, we denote all parameters with θ), and $Z(\theta) = \int \exp(E_\theta(f_\theta(\mathbf{x}))) d\mathbf{x}$ is the partition function. With this definition of Z , we have $p_\theta(\mathbf{x}) = \tilde{p}_\theta(\mathbf{x}) = \exp(E_\theta(f_\theta(\mathbf{x}))) / Z(\theta)$, a proper density function that represents the distribution of input data. In this work, we implement the energy function with a CNN that takes an image as input and returns a scalar.

The computation of the partition function $Z(\theta)$ is usually intractable. The standard maximum likelihood approach cannot therefore be applied directly to train the model. Instead, we can use gradient-based optimization using the derivative of the log-likelihood of a sample \mathbf{x} (see Appendix A for the full derivation):

$$\frac{\partial \log p_\theta(\mathbf{x})}{\partial \theta} = \frac{\partial E_\theta(f_\theta(\mathbf{x}))}{\partial \theta} - \mathbb{E}_{\mathbf{x}' \sim p_\theta(\mathbf{x}')} \left[\frac{\partial E_\theta(f_\theta(\mathbf{x}'))}{\partial \theta} \right], \quad (3)$$

where \mathbf{x}' is sampled from the model distribution. Recent works [20, 58] have proposed to estimate this gradient with MCMC sampling (Markov Chain Monte Carlo). Using a number of K samples, this gives:

$$\frac{\partial \log p_\theta(\mathbf{x})}{\partial \theta} \approx \frac{\partial E_\theta(f_\theta(\mathbf{x}))}{\partial \theta} - \frac{1}{K} \sum_k \frac{\partial E_\theta(f_\theta(\mathbf{x}'_k))}{\partial \theta}, \quad (4)$$

In this estimation, a single sample is typically obtained using Langevin dynamics [72] from p_θ as follows:

$$\mathbf{x}'_{k,t} = \mathbf{x}'_{k,t-1} + \frac{\lambda}{2} \frac{\partial E_\theta(f_\theta(\mathbf{x}'_{k,t-1}))}{\partial \mathbf{x}'_k} + \omega_t, \quad (5)$$

with $\mathbf{x}'_{k,t}$ denoting the t th iteration in the Markov chain for generating the k th instance, λ being the step size, $\omega_t \sim \mathcal{N}(0, \lambda)$, and $\mathbf{x}'_{k,0}$ initialized as uniform random noise. The procedure defines a distribution q_θ such that, if $t \rightarrow \infty$ and $\lambda \rightarrow 0$, then $q_\theta \rightarrow p_\theta$ [72]. In practice, we differentiate only through the last step to reduce the computational cost as in [19]. The model is trained with a contrastive divergence objective [37]. This minimizes the energy of the training data and maximizes that of the generated samples, as illustrated in Figure 1. The alternatives for training EBM where the normalizer is approximated using a generator network is proposed in [1] that helps mitigate part of these practical limitations.

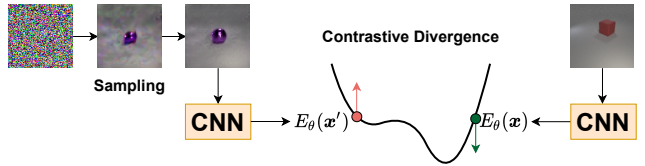


Figure 1. High-level illustration of the training of an EBM.

3.3. Contrastive learning

Contrastive learning (CL) is another self-supervised technique whose core idea is to learn data representations such that similar samples are grouped together and dissimilar ones are pushed apart. In the absence of ground-truth annotations, all training examples are considered “dissimilar” from one another. “Similar” pairs are obtained by generating several views of each example with data augmentations

(i.e. hard-coded transformations that do not affect the semantic contents of the image). The key components of CL are (1) the data augmentations, (2) the encoding function mapping pixels to the embedding space, and (3) the contrastive loss that maximizes the similarity between encodings of similar pairs and minimizes that of dissimilar ones, as illustrated in Figure 2.

On a high level, CL proceeds as follows. Each training example x is transformed with two sets of augmentations into a pair of views \tilde{x} and \tilde{x}' . They are passed through an encoding function such as a CNN to obtain representations. These form a *positive* pair, while combinations of views from different examples form *negative* pairs. The training objective then maximizes the similarity of positive pairs while minimizing that of negative ones. A common implementation of this objective is the normalized temperature-scaled cross-entropy loss over the cosine similarity of representations:

$$\text{score}(\tilde{x}, \tilde{x}') = \frac{f_{\theta}(\tilde{x})^{\top} f_{\theta}(\tilde{x}')}{\tau \|f_{\theta}(\tilde{x})\| \|f_{\theta}(\tilde{x}')\|}, \quad (6)$$

where τ is a temperature hyperparameter. Further,

$$Z_{\text{CL}}(\theta) = \sum_k^K \exp(\text{score}(f_{\theta}(\tilde{x}), f_{\theta}(\tilde{x}_k))) \quad x \neq x_k.$$

Here, x_k samples are usually chosen to be paired with the current mini-batch during SGD. The overall loss is the sum over all positive pairs in the current mini-batch.

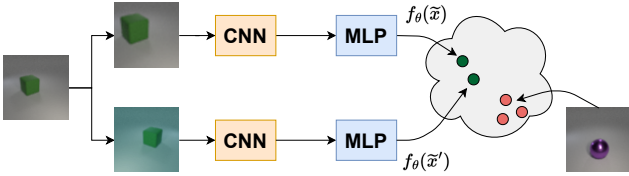


Figure 2. High-level illustration of contrastive learning.

3.4. VQA Model

In our main experiments we use a simple VQA model that is built from a pretrained visual encoder as follows. We combine a visual encoder f^I (a CNN) with a question encoder f^Q (an LSTM). They respectively process an image x^I and question x^Q into representations $v \in \mathbb{R}^{D_I}$ and $q \in \mathbb{R}^{D_Q}$:

$$v = f_{\theta}^I(x^I) \quad \text{and} \quad q = f_{\theta}^Q(x^Q) \quad (7)$$

These are concatenated into a single vector $p = [v, q]$, $p \in \mathbb{R}^{D_I + D_Q}$. This vector is passed through an MLP classifier to obtain answer scores $y = f^{CLS}(p)$, with $y \in \mathbb{R}^A$ where A is the size of a set of candidate answers. The model is trained with supervision on question/image/answer triplets

to minimize a cross-entropy loss:

$$\text{softmax}(y_i) = \frac{\exp(y_i)}{\sum_{j=1}^A \exp(y_j)}, \quad (8)$$

$$\mathcal{L}_{CE} = - \sum_{i=1}^A \hat{a}_i \cdot \log(\text{softmax}(y_i)), \quad (9)$$

where $\hat{a} \in \{0, 1\}^A$ denotes the one-hot (multi-hot) vector of the ground-truth answer(s), and i indexes vector elements.

4. Our implementation

Our VQA model is a simple CNN–LSTM architecture, commonly used as a baseline in early work on VQA [3, 54, 61]. We settled on this simple option because it reduces the training instabilities arising when training EBMs within more complex architectures [19, 20]. The CNN in this architecture is the EBM version of a ResNet [31] from Du *et al.* [19]. The same ResNet backbone is used in all pretraining and fine-tuning experiments to enable transfer learning. We only modify its last few layers for each pretraining task, as discussed below.

For EBM pretraining, we append the CNN model with a linear layer producing a scalar energy value. To facilitate the training we incorporate three changes proposed by Du *et al.* [19]. (1) We use a replay buffer to store previously generated samples that are randomly chosen to reinitialize the sampling chain (Equation 5) instead of the uniform noise. (2) We apply random data augmentations (cropping, horizontal flipping, blurring, and color distortions) to images sampled from the buffer, which improves the diversity and mixing of the sampling chain. (3) We include additional losses that improve the contrastive-divergence training (see [19] for details).

For contrastive pretraining, we use the popular SimCLR method [10]. The standard SimCLR uses a standard ResNet-50 to extract visual representations and an additional projection head into the space where the contrastive loss is applied. We swap the ResNet-50 for the one mentioned above and keep the standard projection head (a 1-layer MLP with ReLU activations). This model is referred to as SimCLR* to emphasize the modified architecture. We use the same data augmentations as for EBM pretraining.

5. Experiments

Diagnostic dataset. Our main experiments use a custom controlled small-scale dataset, most similar to the existing CLEVR-CoGenT [39]. It similarly allows evaluating systematic generalization to unseen combinations of objects/colors. The reason for a new small-scale dataset is our

Split	Object/color combinations	Nb. of images	Nb. of questions
Pretraining	\mathcal{A}	12,000	—
Training	\mathcal{B}	3,600	3,600
Validation	$\mathcal{B} \cup \mathcal{C}$	800	800
Test	\mathcal{C}	3,600	3,600

(a) Data splits.

	Object	Color
\mathcal{A}	Cylinder	Any.
	Cube	Any.
	Sphere	Any.
\mathcal{B}	Cube	Gray, blue, brown, yellow.
	Sphere	Red, green, purple, cyan.
\mathcal{C}	Cube	Red, green, purple, cyan.
	Sphere	Gray, blue, brown, yellow.

(b) Sets of object/color combinations.

Table 1. Summary of our diagnostic dataset. The pretraining, fine-tuning, and test splits contain different object/color combinations.

desire to evaluate EBM, which remain computationally expensive at the time of this study (mid 2021). Contemporary work on EBMs [18, 24] indeed focuses on small datasets like MNIST [16], CIFAR [46] and CelebA [53].

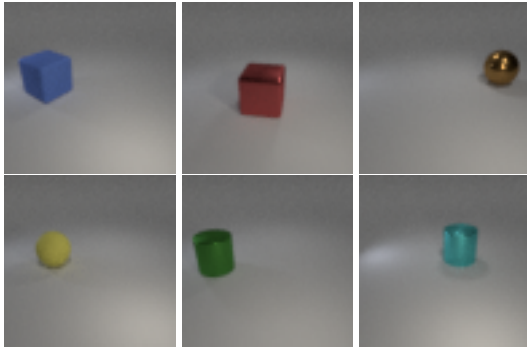


Figure 3. Example images from our diagnostic dataset. Questions are designed to query the object’s shape. For example, for the first image: *There is a blue object in the image; what is it?*, with the correct answer being *cube*.

We generate our dataset following the procedure of [5]. We render 64×64 images with Blender [13]. Each image contains one of three objects (sphere, cube, or cylinder) in one of eight colors (red, purple, yellow, blue, green, cyan, gray, or brown). For each object/color combination, we generate 2000 samples, randomizing the object size, material (rubber or metallic), position, and lightning. We assign disjoint subsets of object/color combinations to the pretraining, fine-tuning, and evaluation sets, as summarized in

Table 1. The validation set contains a mix of in-domain (ID) and out-of-distribution (OOD) data, while the test set is fully OOD. The validation set serves to select hyperparameters and perform early stopping.

For each image, we use templates from CLEVR to generate a question that queries the object shape (*e.g.* *There is a blue object in the image; what is it?*, with the three possible answers *sphere*, *cube* and *cylinder*). Because the range of questions is limited, **the input questions are in fact not necessary for a VQA model to find the correct answer. However they act as distractors since they are spuriously correlated with the correct answers** because of mentioning colors. A model relying on these spurious correlations would however perform badly on our test set because of the novel object/color combinations. See Figure 3 for examples.

5.1. Generalization without/with pretraining

We report our main results in Table 2. We compare models built with an EBM- or CL-pretrained vision encoder, with a baseline that is not pretrained, *i.e.* only trained with supervision on the VQA data. The baseline overfits to the particular object/color combinations of the VQA data and is therefore unable to generalize to the novel combinations of the validation (ID+OOD data) nor test splits (fully OOD data). Of our pretrained models, **the CL method (SimCLR*) achieves the highest, near-perfect accuracy of 99.26% on the test set.** It seems to better disentangle the representations of shape from color, such that the VQA model can generalize to new combinations at test time without overfitting to the particular combinations seen during training. EBM pretraining also improves generalization (86.74% on the test set) but with a high variance across runs (standard deviation of 8.34%). SimCLR* shows no such stability issues (standard deviation of 0.29%).

We also evaluate a model with ImageNet-pretrained ResNet-18 as the visual encoder, which is the most common paradigm for pretraining via transfer learning. However the comparison is relatively unfair to our self-supervised models since this model relies on vastly more pretraining data as well as the ImageNet labels. Still, SimCLR* performs on par with this model.

We also experimented with using our pretrained visual encoders frozen within a VQA model. These results were always worse than with fine-tuning and are not included in the tables.

5.2. Amount of pretraining data

To better understand the benefits of pretraining in low-data regimes, we repeat our experiments while decreasing

	Validation	Test		
	Overall	Overall	Cube only	Sphere only
Baseline without visual pretraining	56.96 \pm 6.08	12.78 \pm 9.75	0.04 \pm 0.06	25.52 \pm 19.57
Baseline with supervised ImageNet pretraining	99.43 \pm 0.33	99.14 \pm 0.20	98.35 \pm 0.33	99.92 \pm 0.09
With self-supervised pretraining: EBM	93.67 \pm 3.18	86.74 \pm 8.34	96.57 \pm 1.99	76.91 \pm 14.75
With self-supervised pretraining: SimCLR*	99.75 \pm 0.33	99.26 \pm 0.29	98.87 \pm 0.27	99.65 \pm 0.32

Table 2. Main results (average accuracy in % \pm one standard deviation over 3 random seeds). The baseline overfits to spurious correlations in the training data and performs poorly on the OOD validation and test sets. The EBM pretraining improves generalization, but SimCLR* performs significantly better and achieves near-perfect accuracy.

the amount of pretraining data (unlabeled images) or labeled training data (VQA examples). See Figures 4–5.

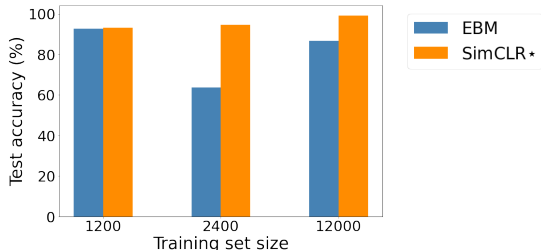


Figure 4. **Decreasing the amount of pretraining data.** The performance of SimCLR* model degrades only slightly even down to a 10-fold decrease. SimCLR* also remains superior to EBM in all regimes. The training stability of EBM proves again to be a challenge. The high variability across runs even shows up as a slight improvement in performance with less pretraining data, although this is an artifact of these instabilities.

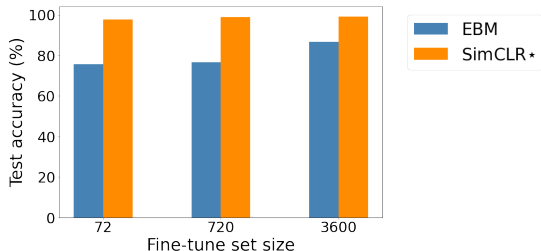


Figure 5. **Decreasing the amount of labeled data.** Both CL and EBM pretraining enable training the VQA model with very little data, even as few as 72 examples. The accuracy of EBM drops only slightly, and that of SimCLR* model remains almost identical.

5.3. Out-of-distribution detection

OOD Detection is relevant to VQA because it can help determine whether a given image/question is answerable [7, 12]. An image of low quality or from a different domain than the training examples (*e.g.* clip art vs. photographs) can be detected as OOD and warn the user that the VQA model may not be reliable on this particular input.

A common baseline for OOD detection with a discriminative model (such as our VQA model pretrained with CL) is to compare the top softmax score with a predefined threshold. A low score means a low confidence hence an OOD sample [35]. EBMs have been purported to be useful for OOD detection [21, 52] by their generative nature since they specifically model the distribution of the training data. To use EBMs for OOD detection, one can simply compare the negative energy estimated by the model with a threshold.

Experimental setup. We evaluate our EBM and CL visual encoders from Section 5.1. As ID test data, we use the images from the test set of our toy VQA task. As OOD data, we use images from various existing datasets (CIFAR [46], MNIST [16], SVHN [56], and VQA v2 [23]) as well as images of random noise, of cone shapes (of similar style as the toy VQA data), and of empty backgrounds (see Figure 6). We compare our SimCLR* and EBM models using their softmax score and negative energy, respectively, for OOD detection. To quantify detection performance across possible thresholds, we compute the area under the ROC curve (AUROC).

Results. On five out of our seven datasets, EBMs are superior to CL (see Table 3). They can distinguish ID from OOD data almost perfectly (AUROC of ~ 1.0). However, when the OOD data is visually similar to the training data (*e.g.* images of backgrounds and cones), the detection performance of our EBM falls well below CL. **The estimated energies appear generally reliable for filtering out OOD samples, but they seem less able to spot fine-grained differences.** See also Figure 7 for the distributions of scores over different datasets.

5.4. Supervised energy-based training

This section looks at energy-based methods for training the VQA model itself *i.e.* not solely the visual encoder. In our experiments so far, EBMs have proved generally inferior to CL. This section investigates whether other purported capabilities of EBMs have value for VQA.

	Source of OOD test data						
	Noise	CIFAR	MNIST	SVHN	VQA v2	Background	Cones
EBM	$\sim\mathbf{1.00}$	$\sim\mathbf{1.00}$	$\sim\mathbf{1.00}$	$\sim\mathbf{1.00}$	$\sim\mathbf{1.00}$	0.52	0.30
SimCLR*	0.96	0.92	0.97	0.91	0.94	0.94	0.82

Table 3. OOD Detection experiment. The AUROC is near-perfect (~ 1.0) for our EBM model on most test sets. However, it falls well below our CL model when the OOD test data is visually similar to the training (ID) data (last two columns).

	Answer accuracy (%)				Calibration
	Overall	Spheres	Cubes	Cylinders	ECE (%)
	(Seen combinations)	(Seen combinations)	(OOD object/color combinations)	(OOD object/color combinations)	(Lower is better)
Random guessing	33.34	33.34	33.34	33.34	—
Baseline, cross-entropy classification objective	33.34	100.00	0.00	0.00	71.54
Standard JEM [24]	29.98	99.93	0.00	0.00	71.28
Modified JEM: downscaled classification loss & early stopping	49.10	99.93	39.23	8.12	36.55
CEBM [19]	35.75	54.60	31.56	21.10	9.24

Table 4. Supervised energy-based training of a VQA model. Modified JEM correctly classifies some of the OOD samples and improves calibration over the standard classification baseline. However, its performance is still far below optimal.

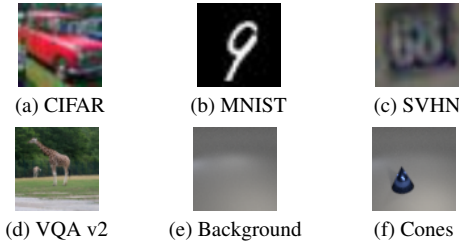


Figure 6. Test examples used in our OOD detection experiment.

We look in particular at (1) their ability to simultaneously address generative and discriminative tasks and (2) their improved calibration compared to standard discriminative models. We test two existing energy-based methods to train the VQA model with supervision from standard question/image/answer triplets.

Setup. We use a dataset similar to Section 5 that allows evaluating ID and OOD accuracy. Every image/question contains either a sphere, a cube, or a cylinder. Spheres can be of any color (ID test data), whereas the sets of possible colors of cubes and cylinders are disjoint and swapped between training and test (OOD data). Our baseline is the same CNN-LSTM as mentioned in Section 4. The JEM and CEBM methods build on this same architecture. We briefly review these methods before presenting our results.

The JEM approach [24] treats a discriminative classifier as an energy-based model by optimizing a double objective:

$$\log p_{\theta}(\mathbf{x}, y) = \log p_{\theta}(\mathbf{x}) + \log p_{\theta}(y|\mathbf{x}), \quad (10)$$

where \mathbf{x} is a training point and y is its class label. This objective can be optimized with standard cross-entropy for classification part and log-likelihood (Equation 4) for energy learning. The energy function is defined as the negative LogSumExp(\cdot) function of the logits of the classifier:

$$E_{\theta}(\mathbf{x}) = -\log \sum_y \exp(f_{\theta}(\mathbf{x})[y]). \quad (11)$$

The CEBM approach [19, 20] learns a conditional energy function $E_{\theta}(\mathbf{x}|c)$. Although CEBMs are mainly designed for image generation, they have also shown solid classification performance [20] by using the class-conditioned energy of an image to predict its label:

$$y^* = \arg \min_y E_{\theta}(\mathbf{x}|y). \quad (12)$$

The generative objective of CEBMs lacks a clear stopping criterion. During training, we monitor the model’s FID score [36] and halt the optimization when the FID becomes stable and reaches a value indicating that generated images are visually similar to the training data.

Calibration of uncertainty. We also propose to look at the models’ calibration since this was previously shown to be improved by energy-based training [24, 32]. A model is considered well-calibrated if its confidence (e.g. top softmax score) is higher for correct predictions than incorrect ones. We use the standard *expected calibration error* (ECE) metric [26]. To compute the ECE, one splits the predictions into M bins according to their confidence, and measures the weighted average of the difference between accuracy and

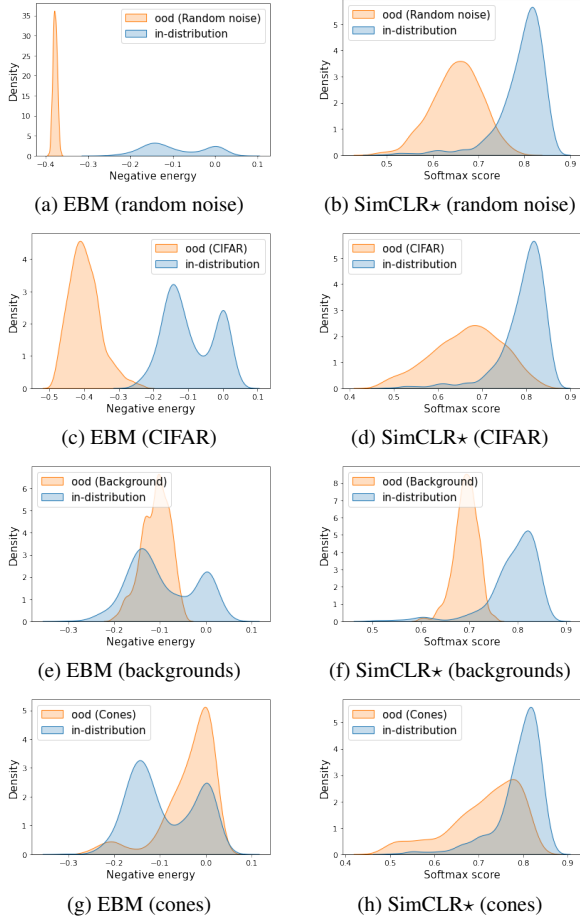


Figure 7. OOD Detection experiment. Distributions of energy and softmax scores, respectively from an EBM (left column) and a SimCLR* model (right column) with test data from various sources (rows). EBMs allow separating ID from OOD data almost perfectly by simple thresholding on some datasets (a,c). However they do poorly when ID and OOD data are visual similar (e,g).

confidence of each bin as follows:

$$\begin{aligned} \text{acc}(B_m) &= (1 / |B_m|) \sum_{i \in B_m} 1(\hat{y}_i = y_i) \\ \text{conf}(B_m) &= (1 / |B_m|) \sum_{i \in B_m} \hat{p}_i \\ \text{ECE} &= \sum_{m=1}^M (|B_m|/n) |\text{acc}(B_m) - \text{conf}(B_m)| \end{aligned} \quad (13)$$

where B_m is the set of indices in bin m , n is the total number of instances, y_i and \hat{y}_i are the predicted and ground truth labels for instance i , and \hat{p}_i is the individual confidence (*e.g.* softmax score) for instance i . An ECE of 0 indicates perfect calibration *i.e.* $p_i = 1$ for correct predictions and 0 for incorrect ones.

Results of supervised energy-based training. The baseline model (Table 4, second row) unsurprisingly overfits the object/color combinations of the training data and is therefore unable to generalize to novel combinations at test time. The model obtains an accuracy of 100% on questions about

spheres (same combinations in training and test) but 0% on cubes and cylinders (OOD combinations). The calibration is also poor (high ECE of 71.54%) indicating that the model is confident about its wrong predictions.

The standard JEM (Table 4, third row) shows poor accuracy and calibration similar to the baseline. Careful inspection revealed that the classification objective quickly dominates the energy learning. In other words, the model could not simultaneously predict correct answers and be capable of generating new images. The classification loss would typically converge much faster and, to minimize the energy loss, the model would start generating non-realistic images that always give a high energy. The energy learning objective is thus ineffective in this regime. We mitigate the dominance of the classification objective by down-scaling the corresponding term by a constant factor (0.1 proved effective). The resulting model then learns to produce naturally-looking images (see Figure 8, bottom row). Nevertheless, at some point during training, we always observed that the model would start generating noisy images that quickly diverge from the training data (see Figure 8, top row). We solve this issue with early stopping, which we trigger when the energies of real and generated images diverge past a threshold: $|E_\theta(x') - E_\theta(x)| > 0.8$.

The modified JEM (Table 4, fourth row) gives a higher overall accuracy (49.10%) as well as a better calibration (ECE of 36.55%). Contrary to the baseline, this model can therefore correctly handle some of the OOD data, although it still often confuses cubes and cylinders with relatively high confidence.

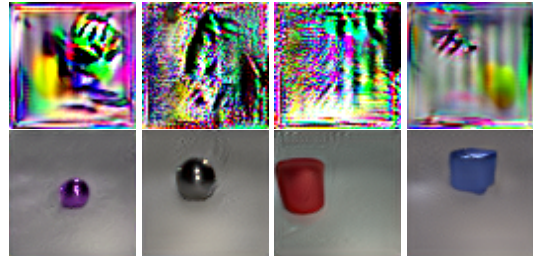


Figure 8. Generated images of high (top) and low energy (bottom).

The CEBM seems to surpass the baseline, but its results are in fact not much better than random predictions. Indeed, even though the CEBM does not overfit to the spurious correlations in the training data like the baseline, but it also fails to correctly answer questions about spheres (the ID test data), which were handled perfectly by the baseline and the JEM. Moreover, we observed a surprising lack of correlation between the CEBM’s FID score (*i.e.* its generative performance, which we use for early stopping) and its VQA accuracy (*i.e.* its discriminative performance). In fact,

the answers predicted by the model fluctuate wildly across epochs. The low ECE score of the CEBM (9.24%) is simply due a low confidence for all (mostly wrong) predictions. Thus it does not correspond to a desirable behavior.

6. Conclusions

The first part of this paper explored the applicability of self-supervised learning to pretrain visual representations for VQA. We experimented with two instantiations of contrastive learning (CL) and energy-based models (EBMs). With both, we could learn representations from unlabeled images that proved effective in a toy VQA setting. After pretraining, the VQA models could be trained with little annotated data and handle OOD instances to some extent. However, we found EBMs to be difficult to put into practice because of unstable training and variability in their results. On the opposite, CL proved much more practical. In our setting, representations learned with CL on little data could compete with those from a supervised, ImageNet-pretrained model.

Overall, self-supervised pretraining is an increasingly attractive alternative to traditional transfer learning from a supervised model. This option is particularly relevant when dealing with particular visual domains *e.g.* for medical VQA [33, 47].

In the second part of this paper, we investigated various purported benefits of EBMs (OOD detection, supervised energy-based training, calibration). These experiments were unfortunately largely negative. This study is limited by the implementation choices that were necessarily made, and by our simplistic evaluation setting – admittedly a far cry from open-domain VQA. Still, our experience suggests that the state of the art on EBMs at the time of this study (mid 2021) is not ready for complex tasks like VQA. Other choices and future developments may of course affect this recommendation.

References

- [1] M. Ehsan Abbasnejad, Qinfeng Shi, Anton van den Hengel, and Lingqiao Liu. A generative adversarial density estimator. In *2019 IEEE/CVF Conference on Computer Vision and Pattern Recognition (CVPR)*, pages 10774–10783, 2019. [3](#)
- [2] Peter Anderson, Xiaodong He, Chris Buehler, Damien Teney, Mark Johnson, Stephen Gould, and Lei Zhang. Bottom-up and top-down attention for image captioning and visual question answering. In *Proceedings of the IEEE Conference on Computer Vision and Pattern Recognition*, volume 3, page 6, 2018. [1](#), [2](#)
- [3] Stanislaw Antol, Aishwarya Agrawal, Jiasen Lu, Margaret Mitchell, Dhruv Batra, C Lawrence Zitnick, and Devi Parikh. Vqa: Visual question answering. In *CVPR*, pages 2425–2433, 2015. [4](#)
- [4] Michael Arbel, Liang Zhou, and Arthur Gretton. Generalized energy based models. In *International Conference on Learning Representations*, 2020. [2](#)
- [5] Yuval Atzmon, Felix Kreuk, Uri Shalit, and Gal Chechik. A causal view of compositional zero-shot recognition. *arXiv preprint arXiv:2006.14610*, 2020. [5](#)
- [6] Philip Bachman, R Devon Hjelm, and William Buchwalter. Learning representations by maximizing mutual information across views. *Advances in Neural Information Processing Systems*, 32:15535–15545, 2019. [2](#)
- [7] Nilavra Bhattacharya, Qing Li, and Danna Gurari. Why does a visual question have different answers? In *CVPR*, pages 4271–4280, 2019. [6](#)
- [8] Zhaowei Cai, Gukyeon Kwon, Avinash Ravichandran, Erhan Bas, Zhuowen Tu, Rahul Bhotika, and Stefano Soatto. X-DETR: A versatile architecture for instance-wise vision-language tasks. *arXiv preprint arXiv:2204.05626*, 2022. [2](#)
- [9] Mathilde Caron, Ishan Misra, Julien Mairal, Priya Goyal, Piotr Bojanowski, and Armand Joulin. Unsupervised learning of visual features by contrasting cluster assignments. In *Thirty-fourth Conference on Neural Information Processing Systems (NeurIPS)*, 2020. [2](#)
- [10] Ting Chen, Simon Kornblith, Mohammad Norouzi, and Geoffrey Hinton. A simple framework for contrastive learning of visual representations. In *ICML*, pages 1597–1607. PMLR, 2020. [2](#), [3](#), [4](#)
- [11] Yen-Chun Chen, Linjie Li, Licheng Yu, Ahmed El Kholy, Faisal Ahmed, Zhe Gan, Yu Cheng, and Jingjing Liu. Uniter: Universal image-text representation learning. In *Proceedings of the European Conference on Computer Vision*, 2020. [1](#)
- [12] Tai-Yin Chiu, Yanan Zhao, and Danna Gurari. Assessing image quality issues for real-world problems. In *Proceedings of the IEEE Conference on Computer Vision and Pattern Recognition*, pages 3646–3656, 2020. [6](#)
- [13] Blender Online Community. *Blender - a 3D modelling and rendering package*. Blender Foundation, Stichting Blender Foundation, Amsterdam, 2018. [5](#)
- [14] Corentin Dancette, Remi Cadene, Damien Teney, and Matthieu Cord. Beyond question-based biases: Assessing multimodal shortcut learning in visual question answering. In *Proceedings of the IEEE/CVF International Conference on Computer Vision*, pages 1574–1583, 2021. [1](#)
- [15] Jia Deng, Wei Dong, Richard Socher, Li-Jia Li, Kai Li, and Li Fei-Fei. Imagenet: A large-scale hierarchical image database. In *Proceedings of the IEEE Conference on Computer Vision and Pattern Recognition*, pages 248–255, 2009. [2](#)
- [16] Li Deng. The mnist database of handwritten digit images for machine learning research. *IEEE Signal Processing Magazine*, 29(6):141–142, 2012. [5](#), [6](#)
- [17] Yuntian Deng, Anton Bakhtin, Myle Ott, Arthur Szlam, and Marc’Aurelio Ranzato. Residual energy-based models for text generation. In *International Conference on Learning Representations*, 2019. [2](#)

- [18] Yilun Du, Shuang Li, and Igor Mordatch. Compositional visual generation with energy based models. *Advances in Neural Information Processing Systems*, 33:6637–6647, 2020. 2, 5
- [19] Yilun Du, Shuang Li, Joshua Tenenbaum, and Igor Mordatch. Improved contrastive divergence training of energy based models. *arXiv preprint arXiv:2012.01316*, 2020. 2, 3, 4, 7
- [20] Yilun Du and Igor Mordatch. Implicit generation and modeling with energy based models. *Advances in Neural Information Processing Systems*, 32:3608–3618, 2019. 2, 3, 4, 7
- [21] Sven Elfle, Bertrand Charpentier, Daniel Zügner, and Stephan Günnemann. On out-of-distribution detection with energy-based models. *arXiv preprint arXiv:2107.08785*, 2021. 6
- [22] Ian Goodfellow, Jean Pouget-Abadie, Mehdi Mirza, Bing Xu, David Warde-Farley, Sherjil Ozair, Aaron Courville, and Yoshua Bengio. Generative adversarial nets. *Advances in neural information processing systems*, 27, 2014. 1
- [23] Yash Goyal, Tejas Khot, Douglas Summers-Stay, Dhruv Batra, and Devi Parikh. Making the v in VQA matter: Elevating the role of image understanding in visual question answering. In *Proceedings of the IEEE Conference on Computer Vision and Pattern Recognition*, pages 6904–6913, 2017. 6
- [24] Will Grathwohl, Kuan-Chieh Wang, Joern-Henrik Jacobsen, David Duvenaud, Mohammad Norouzi, and Kevin Swersky. Your classifier is secretly an energy based model and you should treat it like one. In *International Conference on Learning Representations*, 2019. 2, 5, 7
- [25] Liangke Gui, Qiuyuan Huang, Alex Hauptmann, Yonatan Bisk, and Jianfeng Gao. Training vision-language transformers from captions alone. *arXiv preprint arXiv:2205.09256*, 2022. 2
- [26] Chuan Guo, Geoff Pleiss, Yu Sun, and Kilian Q Weinberger. On calibration of modern neural networks. In *ICML*, pages 1321–1330. PMLR, 2017. 7
- [27] Fredrik Gustafsson, Martin Danelljan, Radu Timofte, and Thomas B Schön. How to train your energy-based model for regression. In *Proceedings of the British Machine Vision Conference*, 2020. 2
- [28] Fredrik K Gustafsson, Martin Danelljan, Goutam Bhat, and Thomas B Schön. Energy-based models for deep probabilistic regression. In *Proceedings of the European Conference on Computer Vision*, pages 325–343. Springer, 2020. 2
- [29] Tian Han, Erik Nijkamp, Xiaolin Fang, Mitch Hill, Song-Chun Zhu, and Ying Nian Wu. Divergence triangle for joint training of generator model, energy-based model, and inferential model. In *Proceedings of the IEEE Conference on Computer Vision and Pattern Recognition*, pages 8670–8679, 2019. 2
- [30] Kaiming He, Haoqi Fan, Yuxin Wu, Saining Xie, and Ross Girshick. Momentum contrast for unsupervised visual representation learning. In *Proceedings of the IEEE Conference on Computer Vision and Pattern Recognition*, pages 9729–9738, 2020. 2
- [31] Kaiming He, Xiangyu Zhang, Shaoqing Ren, and Jian Sun. Deep residual learning for image recognition. In *Proceedings of the IEEE Conference on Computer Vision and Pattern Recognition*, pages 770–778, 2016. 1, 4
- [32] Tianxing He, Bryan McCann, Caiming Xiong, and Ehsan Hosseini-Asl. Joint energy-based model training for better calibrated natural language understanding models. In *Proceedings of the Conference of the European Chapter of the Association for Computational Linguistics*, pages 1754–1761, 2021. 2, 7
- [33] Xuehai He, Yichen Zhang, Luntian Mou, Eric Xing, and Pengtao Xie. Pathvqa: 30000+ questions for medical visual question answering. *arXiv preprint arXiv:2003.10286*, 2020. 9
- [34] Olivier Henaff. Data-efficient image recognition with contrastive predictive coding. In *ICML*, pages 4182–4192. PMLR, 2020. 2
- [35] Dan Hendrycks and Kevin Gimpel. A baseline for detecting misclassified and out-of-distribution examples in neural networks. *arXiv preprint arXiv:1610.02136*, 2016. 6
- [36] Martin Heusel, Hubert Ramsauer, Thomas Unterthiner, Bernhard Nessler, and Sepp Hochreiter. Gans trained by a two time-scale update rule converge to a local nash equilibrium. *Advances in Neural Information Processing Systems*, 30, 2017. 7
- [37] Geoffrey E Hinton. Training products of experts by minimizing contrastive divergence. *Neural computation*, 14(8):1771–1800, 2002. 3
- [38] Zhicheng Huang, Zhaoyang Zeng, Yupan Huang, Bei Liu, Dongmei Fu, and Jianlong Fu. Seeing out of the box: End-to-end pre-training for vision-language representation learning. In *Proceedings of the IEEE Conference on Computer Vision and Pattern Recognition*, 2021. 2
- [39] Justin Johnson, Bharath Hariharan, Laurens van der Maaten, Li Fei-Fei, C Lawrence Zitnick, and Ross Girshick. Clevr: A diagnostic dataset for compositional language and elementary visual reasoning. In *Proceedings of the IEEE Conference on Computer Vision and Pattern Recognition*, 2017. 1, 4
- [40] Kushal Kafle and Christopher Kanan. Visual question answering: Datasets, algorithms, and future challenges. *Computer Vision and Image Understanding*, 163:3–20, 2017. 1
- [41] Kushal Kafle, Robik Shrestha, and Christopher Kanan. Challenges and prospects in vision and language research. *Frontiers in Artificial Intelligence*, 2:28, 2019. 1
- [42] Aishwarya Kamath, Mannat Singh, Yann LeCun, Gabriel Synnaeve, Ishan Misra, and Nicolas Carion. MDETR-modulated detection for end-to-end multi-modal understanding. In *Proceedings of the IEEE Conference on Computer Vision and Pattern Recognition*, pages 1780–1790, 2021. 2
- [43] Wonjae Kim, Bokyoung Son, and Ildoo Kim. ViLT: Vision-and-language transformer without convolution or region supervision. In *ICML*, pages 5583–5594. PMLR, 2021. 2
- [44] Diederik P Kingma and Max Welling. Auto-encoding variational bayes. *arXiv preprint arXiv:1312.6114*, 2013. 1
- [45] Ranjay Krishna, Yuke Zhu, Oliver Groth, Justin Johnson, Kenji Hata, Joshua Kravitz, Stephanie Chen, Yannis Kalanidis, Li-Jia Li, David A Shamma, and Others. Visual

- genome: Connecting language and vision using crowd-sourced dense image annotations. *International Journal of Computer Vision*, 123(1):32–73, 2017. 2
- [46] Alex Krizhevsky, Geoffrey Hinton, et al. Learning multiple layers of features from tiny images. 2009. 5, 6
- [47] Jason J Lau, Soumya Gayen, Asma Ben Abacha, and Dina Demner-Fushman. A dataset of clinically generated visual questions and answers about radiology images. *Scientific data*, 5(1):1–10, 2018. 9
- [48] Yann LeCun, Sumit Chopra, Raia Hadsell, M Ranzato, and F Huang. A tutorial on energy-based learning. *Predicting structured data*, 1(0), 2006. 2
- [49] Liunian Harold Li, Mark Yatskar, Da Yin, Cho-Jui Hsieh, and Kai-Wei Chang. Visualbert: A simple and performant baseline for vision and language. *arXiv preprint arXiv:1908.03557*, 2019. 1
- [50] Shuang Li, Yilun Du, Gido M van de Ven, and Igor Mor-datch. Energy-based models for continual learning. *arXiv preprint arXiv:2011.12216*, 2020. 2
- [51] Xijun Li, Xi Yin, Chunyuan Li, Pengchuan Zhang, Xiaowei Hu, Lei Zhang, Lijuan Wang, Houdong Hu, Li Dong, Furu Wei, et al. Oscar: Object-semantics aligned pre-training for vision-language tasks. In *Proceedings of the European Conference on Computer Vision*, pages 121–137. Springer, 2020. 1
- [52] Weitang Liu, Xiaoyun Wang, John D Owens, and Yixuan Li. Energy-based out-of-distribution detection. *arXiv preprint arXiv:2010.03759*, 2020. 6
- [53] Ziwei Liu, Ping Luo, Xiaogang Wang, and Xiaoou Tang. Deep learning face attributes in the wild. In *CVPR*, 2015. 5
- [54] Mateusz Malinowski, Marcus Rohrbach, and Mario Fritz. Ask your neurons: A neural-based approach to answering questions about images. In *CVPR*, pages 1–9, 2015. 4
- [55] Tomas Mikolov, Kai Chen, Greg Corrado, and Jeffrey Dean. Efficient estimation of word representations in vector space. *arXiv preprint arXiv:1301.3781*, 2013. 1
- [56] Yuval Netzer, Tao Wang, Adam Coates, Alessandro Bis-sacco, Bo Wu, and Andrew Y Ng. Reading digits in natural images with unsupervised feature learning. 2011. 6
- [57] Erik Nijkamp, Mitch Hill, Tian Han, Song-Chun Zhu, and Ying Nian Wu. On the anatomy of mcmc-based maximum likelihood learning of energy-based models. In *Proceedings of the AAAI Conference on Artificial Intelligence*, volume 34, pages 5272–5280, 2020. 2
- [58] Erik Nijkamp, Mitch Hill, Song-Chun Zhu, and Ying Nian Wu. Learning non-convergent non-persistent short-run MCMC toward energy-based model. *arXiv preprint arXiv:1904.09770*, 2019. 2, 3
- [59] Aaron van den Oord, Yazhe Li, and Oriol Vinyals. Representation learning with contrastive predictive coding. *arXiv preprint arXiv:1807.03748*, 2018. 2
- [60] Jeffrey Pennington, Richard Socher, and Christopher Man-ning. Glove: Global vectors for word representation. In *Proceedings of the Conference on Empirical Methods in Natural Language Processing*, pages 1532–1543, 2014. 1
- [61] Mengye Ren, Ryan Kiros, and Richard Zemel. Exploring models and data for image question answering. *Advances in Neural Information Processing Systems*, 28:2953–2961, 2015. 4
- [62] Jan-Martin O Steitz, Jonas Pfeiffer, Iryna Gurevych, and Stefan Roth. TxT: Crossmodal end-to-end learning with transformers. In *DAGM German Conference on Pattern Recognition*, pages 405–420. Springer, 2021. 2
- [63] Mohammed Suhail, Abhay Mittal, Behjat Siddiquie, Chris Broadbuss, Jayan Eledath, Gerard Medioni, and Leonid Sigal. Energy-based learning for scene graph generation. In *Proceedings of the IEEE Conference on Computer Vision and Pattern Recognition*, pages 13936–13945, 2021. 2
- [64] Hao Tan and Mohit Bansal. Lxmert: Learning cross-modality encoder representations from transformers. In *Proceedings of the Conference on Empirical Methods in Natural Language Processing and the International Joint Conference on Natural Language Processing*, pages 5103–5114, 2019. 1, 2
- [65] Damien Teney, Ehsan Abbasnejad, and Anton van den Hen-gel. Learning what makes a difference from counterfactual examples and gradient supervision. In *European Conference on Computer Vision*, pages 580–599. Springer, 2020. 1
- [66] Damien Teney, Ehsan Abbasnejad, and Anton van den Hen-gel. Unshuffling data for improved generalization. *arXiv preprint arXiv:2002.11894*, 2020. 1
- [67] Damien Teney, Ehsan Abbasnejad, Kushal Kafle, Robik Shrestha, Christopher Kanan, and Anton Van Den Hengel. On the value of out-of-distribution testing: An example of goodhart’s law. *Advances in Neural Information Processing Systems*, 33:407–417, 2020. 1
- [68] Damien Teney, Peter Anderson, Xiaodong He, and Anton van den Hengel. Tips and tricks for visual question answering: Learnings from the 2017 challenge. *arXiv preprint arXiv:1708.02711*, 2017. 2
- [69] Damien Teney, Qi Wu, and Anton van den Hengel. Visual question answering: A tutorial. *IEEE Signal Processing Magazine*, 34:63–75, 2017. 2
- [70] Yonglong Tian, Dilip Krishnan, and Phillip Isola. Con-tractive multiview coding. In *Computer Vision–ECCV 2020: 16th European Conference, Glasgow, UK, August 23–28, 2020, Proceedings, Part XI 16*, pages 776–794. Springer, 2020. 2
- [71] Lifu Tu, Richard Yuanzhe Pang, Sam Wiseman, and Kevin Gimpel. Engine: Energy-based inference networks for non-autoregressive machine translation. In *Proceedings of the Annual Meeting of the Association for Computational Lin-guistics*, pages 2819–2826, 2020. 2
- [72] Max Welling and Yee W Teh. Bayesian learning via stochas-tic gradient Langevin dynamics. In *ICML*, pages 681–688. Citeseer, 2011. 3
- [73] Spencer Whitehead, Hui Wu, Heng Ji, Rogerio Feris, and Kate Saenko. Separating skills and concepts for novel visual question answering. In *Proceedings of the IEEE Conference on Computer Vision and Pattern Recognition*, pages 5632–5641, 2021. 2

- [74] Qi Wu, Damien Teney, Peng Wang, Chunhua Shen, Anthony Dick, and Anton van den Hengel. Visual question answering: A survey of methods and datasets. *Computer Vision and Image Understanding*, 2017. 2
- [75] Zhirong Wu, Yuanjun Xiong, Stella X Yu, and Dahua Lin. Unsupervised feature learning via non-parametric instance discrimination. In *Proceedings of the IEEE Conference on Computer Vision and Pattern Recognition*, pages 3733–3742, 2018. 2
- [76] Zhisheng Xiao, Karsten Kreis, Jan Kautz, and Arash Vahdat. Vaebm: A symbiosis between variational autoencoders and energy-based models. In *International Conference on Learning Representations*, 2020. 2, 3
- [77] Jianwen Xie, Yang Lu, Ruiqi Gao, and Ying Nian Wu. Co-operative learning of energy-based model and latent variable model via mcmc teaching. In *Proceedings of the AAAI Conference on Artificial Intelligence*, volume 32, 2018. 2
- [78] Haiyang Xu, Ming Yan, Chenliang Li, Bin Bi, Songfang Huang, Wenming Xiao, and Fei Huang. E2E-VLP: End-to-end vision-language pre-training enhanced by visual learning. *arXiv preprint arXiv:2106.01804*, 2021. 2
- [79] Stephen Zhao, Jörn-Henrik Jacobsen, and Will Grathwohl. Joint energy-based models for semi-supervised classification. In *ICML Workshop on Uncertainty and Robustness in Deep Learning*, 2020. 2
- [80] Chengxu Zhuang, Alex Lin Zhai, and Daniel Yamins. Local aggregation for unsupervised learning of visual embeddings. In *CVPR*, pages 6002–6012, 2019. 2

Appendices

A. Derivation of Equation 3

The log of the EBM objective is:

$$\log(p_{\theta}(\mathbf{x})) = E_{\theta}(f_{\theta}(\mathbf{x})) - \log(Z(\theta)), \quad (14)$$

and the gradient of the normalizer is:

$$\begin{aligned} \frac{\partial}{\partial \theta} \log(Z(\theta)) &= \frac{\partial}{\partial \theta} \log \left(\int \exp(E_{\theta}(f_{\theta}(\mathbf{x}))) d\mathbf{x} \right) \\ &= \frac{\partial}{\partial \theta} \log \left(\int \exp(E_{\theta}(f_{\theta}(\mathbf{x}))) d\mathbf{x} \right) \\ &= \frac{\frac{\partial}{\partial \theta} \left(\int \exp(E_{\theta}(f_{\theta}(\mathbf{x}))) d\mathbf{x} \right)}{\int \exp(E_{\theta}(f_{\theta}(\mathbf{x}))) d\mathbf{x}} \\ &= \frac{\int \frac{\partial}{\partial \theta} \exp(E_{\theta}(f_{\theta}(\mathbf{x}))) d\mathbf{x}}{\int \exp(E_{\theta}(f_{\theta}(\mathbf{x}))) d\mathbf{x}} \\ &= \int \frac{\frac{\partial}{\partial \theta} \exp(E_{\theta}(f_{\theta}(\mathbf{x})))}{\int \exp(E_{\theta}(f_{\theta}(\mathbf{x}))) d\mathbf{x}} d\mathbf{x} \\ &= \int \frac{\frac{\partial}{\partial \theta} E_{\theta}(f_{\theta}(\mathbf{x})) \exp(E_{\theta}(f_{\theta}(\mathbf{x})))}{\int \exp(E_{\theta}(f_{\theta}(\mathbf{x}))) d\mathbf{x}} d\mathbf{x} \\ &= \int \frac{\partial}{\partial \theta} E_{\theta}(f_{\theta}(\mathbf{x})) \frac{\exp(E_{\theta}(f_{\theta}(\mathbf{x})))}{\int \exp(E_{\theta}(f_{\theta}(\mathbf{x}))) d\mathbf{x}} d\mathbf{x} \\ &= \int p_{\theta}(\mathbf{x}) \frac{\partial}{\partial \theta} E_{\theta}(f_{\theta}(\mathbf{x})) \\ &= \mathbb{E}_{\mathbf{x} \sim p_{\theta}(\mathbf{x})} \left[\frac{\partial}{\partial \theta} E_{\theta}(f_{\theta}(\mathbf{x})) \right], \end{aligned} \quad (15)$$

Thus, the gradient of the log probability is:

$$\frac{\partial \log p_{\theta}(\mathbf{x})}{\partial \theta} = \frac{\partial E_{\theta}(f_{\theta}(\mathbf{x}))}{\partial \theta} - \mathbb{E}_{\mathbf{x}' \sim p_{\theta}(\mathbf{x}')} \left[\frac{\partial E_{\theta}(f_{\theta}(\mathbf{x}'))}{\partial \theta} \right], \quad (16)$$